Dalton Transactions

ROYAL SOCIETY OF CHEMISTRY

PAPER

View Article Online
View Journal | View Issue

Check for updates

Cite this: *Dalton Trans.*, 2025, **54**, 13235

Thio-iso-phthalamide pincer ligand-driven oxidative addition of a C–Br bond to gold(I): synthesis and studies of SCS–gold(III) pincer complexes

Saravanan Raju, [a,b] Sanhati Sharangi, [b] Harkesh B. Singh, [a] R. S. Prabhuraj, [c] Rohit Srivastava, [c] Ray J. Butcher [d] and Sangit Kumar *[b]

Received 17th April 2025,
Accepted 29th July 2025

DOI: 10.1039/d5dt00916b

rsc.li/dalton

The chelating effect of thio-iso-phthalamides was utilized to facilitate the oxidative addition of an aryl Csp^2–Br bond into the $SMe_2Au(I)Cl$ salt, leading to the isolation of stable SCS·Au(III)X (X = Br and Cl) complexes. The subsequent displacement of bromide with silver triflate, followed by the addition of phosphine/phosphite ligands, afforded a series of neutral, highly stable organogold(III) complexes. The thioamide pincer ligand acts as a trianionic species due to iminothiolate formation. The isolated complexes were thoroughly characterized by NMR, mass spectrometry, IR spectroscopy, and single-crystal X-ray diffraction techniques. The redox potential of the complexes was measured by cyclic voltammetry, revealing that the reduction of Au(III) to Au(I) to Au(0) is an irreversible redox process. The pathway of gold(III) complex formation was investigated using DFT analysis, which suggested that the bi-chelation of the thioamide groups facilitated the oxidative addition of C–Br bonds to the Au(I) centre.

Introduction

Oxidative addition is a key step in transition metal-catalyzed cross-coupling reactions.[1–11] The oxidative addition of transition metals is well explored on the polar and non-polar sigma bonds, and the related mechanistic studies are well understood.[12] However, the elementary oxidative addition of an aryl bromide bond to gold(I) remained challenging due to the high redox potential of the Au(I)/Au(III) couple compared to its isoelectronic Pd(0)/Pd(II) counterpart, despite having stable +1, +2 and +3 oxidation states.[2,3,13–24]

Initially, gold(I) complexes were considered redox-neutral catalysts. As a result, a stoichiometric amount of external oxidants was required to facilitate oxidation to Au(III) in catalytic reactions.[18,25–27] Recent studies suggest that oxidative addition in gold(I) complexes is influenced by several factors, including the electronic environment, coordination number, geometry, bond strain, and the polarity of Si–Si, Sn–Sn, and C–C bonds.[13,17,28–33]

Furthermore, electron-rich aryl halides exhibit enhanced reactivity toward oxidative addition with Au(I) complexes compared to Pd(0),[34–36] which is attributed to the lower coordination number of gold(I) (CN = 2) relative to the higher coordination number (CN = 4) of palladium(0). Consequently, linear two-coordinated gold(I) complexes are known to effectively activate alkyl $C(sp^3)$–X bonds under mild conditions.

Early studies on oxidative addition in gold(I) complexes

In 1970, Kochi, Puddephatt, and Schmidbaur investigated the oxidative addition of a phosphine gold(I) methyl complex with methyl iodide. This reaction resulted in the formation of ethane and phosphine gold(I) iodide.[37–39] Subsequent studies focused on activating the stronger aryl $C(sp^2)$–Y (Y = leaving group) bond using linear gold(I) complexes.[40–43] In 2007, Corma and co-workers demonstrated that the oxidative addition of phenyl iodide to Me_3PAuI is an endothermic process requiring high activation energy.[44,45] Similarly, O'Hair and colleagues used mass spectrometry and DFT calculations to study $(R_3P)_2Au^+$ complexes (R = Me and Ph). Their findings revealed that these complexes are highly stable and thermodynamically disfavored for oxidative addition of iodobenzene in the gas phase.[46]

Strategies to enhance oxidative addition in gold(I) complexes

To address these challenges, recent years have seen growing interest in tridentate pincer-based complexes, which play a

[a]Department of Chemistry, Indian Institute of Technology Bombay, Mumbai – 400076, Maharashtra, India
[b]Department of Chemistry, Indian Institute of Science Education and Research Bhopal, Bhauri By-pass Road, Bhopal – 462 066, Madhya Pradesh, India
[c]Department of Biosciences and Bioengineering Indian Institute of Technology Bombay, Mumbai – 400076, Maharashtra, India
[d]Department of Chemistry, Howard University, Washington, D.C. 20059, USA

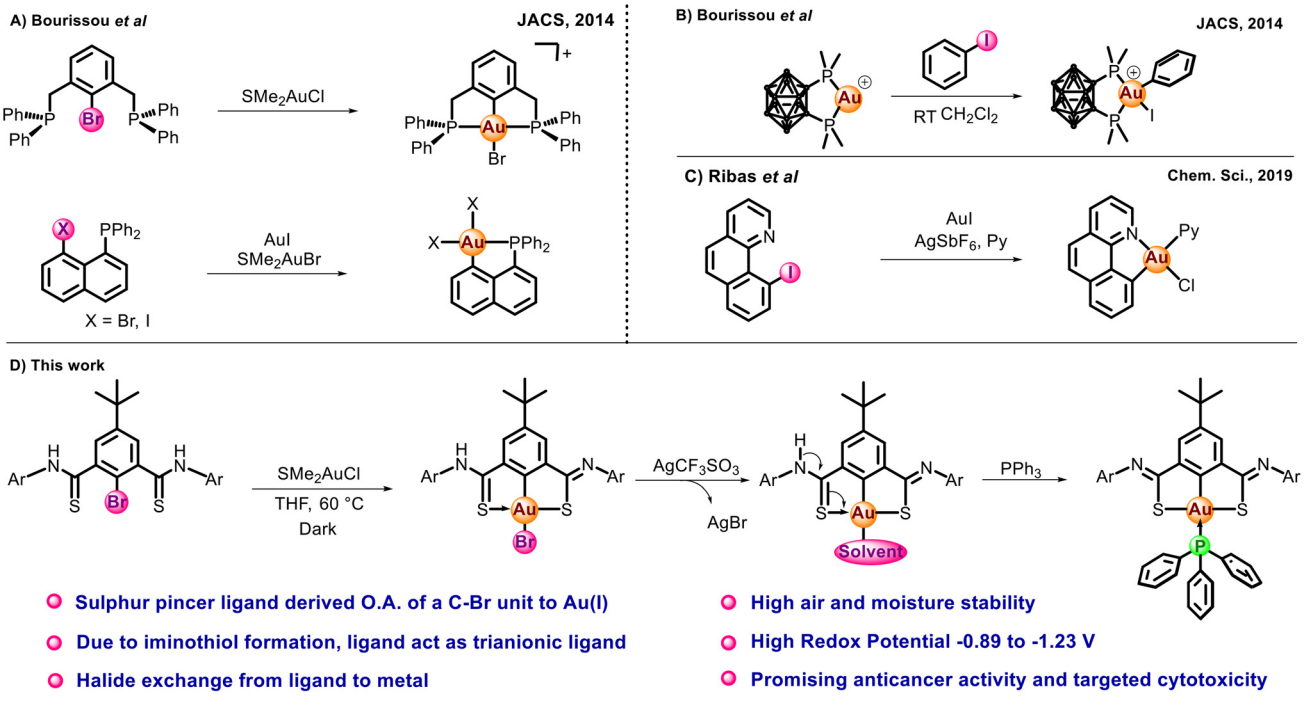

Scheme 1 The chelation-assisted oxidative addition to gold(I) salts.

pivotal role in organometallic chemistry by rigidly anchoring metal centres, thereby providing exceptional stability, tunable electronic properties, and unique reactivities.[47–63] Research on pincer-based complexes was pioneered by Moulton and Shaw in the late 1970s,[64] and the term "pincer" was later coined by van Koten in 1989.[65] Similar strategies have also been utilized in gold chemistry for enhancing the feasibility of oxidative addition in linear gold(I) complexes.[17,28–31,66] Despite this advancement, only a few examples exist where oxidative addition has been successfully performed on aryl halide [C(sp^2)–X] or alkenyl halide [C(sp)–X] bonds.

A breakthrough came in 2014 when Bourissou *et al.* reported phosphine chelation-assisted intramolecular oxidative addition of aryl iodide and bromide to gold(I) complexes (Scheme 1).[67,68] In these systems, intramolecular phosphine bi-chelation brings the gold(I) centre into close proximity to the aryl C(sp^2)–Br bond. This interaction promotes oxidative addition, yielding a cationic [PCP–AuBr]$^+$ complex. Similarly, 8-iodonaphthyl phosphine was identified as a suitable chelating substrate for oxidative addition.[69]

Recent advances in gold(I) oxidative addition reactions

Toste *et al.* demonstrated that NHC–gold(I) cationic complexes can undergo oxidative addition in strained C–C bonds of biphenylenes under mild conditions.[17,70] This is in contrast with other metals, which require harsh conditions for the same transformation.[17,70,71] Ribas and co-workers explored pyridine chelation for oxidative addition in gold(I) complexes. However, their initial attempts using 2-(2-iodophenyl) pyridine were unsuccessful. To address this limitation, they introduced an additional ring to restrict the free rotation of the pyridine ligand. This modification led to the successful oxidative addition of 10-iodobenzo[*h*]quinolone at the aryl C(sp^2)–I bond at 60 °C.[72]

Unexplored areas in gold(I) oxidative addition

Despite these advances, oxidative addition using thio-iso-phthioamide chelation for activating aryl C(sp^2)–Br bonds remains unexplored. Additionally, to the best of our knowledge, neutral, stable, carbophilic thioamide organogold(III) complexes have yet to be isolated.

Our research group previously reported the isolation of organo-Hg, Pd, Pt, Se, and Te complexes using NC$^{(-)}$N-type 5-*tert*-butyl-1,3-bis(benzimidazol-2′-yl)phenyl chelating pincer ligands.[73,74] In this study, we report the isolation of a series of highly stable, neutral, carbophilic thioamide organogold(III) complexes, derived from thio-iso-phthalamide tridentate ligands. Their electronic properties and mechanism of formation have been investigated using DFT calculations.

Results and discussion

Synthesis of pincer gold(III) complexes

The precursor isophthalamides **1** and **2**, used for synthesizing thio-iso-phthalamide ligands **3** and **4**, were prepared in three steps from commercially available 5-*tert*-butyl-*meta*-xylene.[73,75] Subsequently, the amide carbonyl (C=O) groups were converted into thiocarbonyl (C=S) using Lawesson's reagent, yielding yellow crystalline thio-iso-phthalamide ligands **3** and

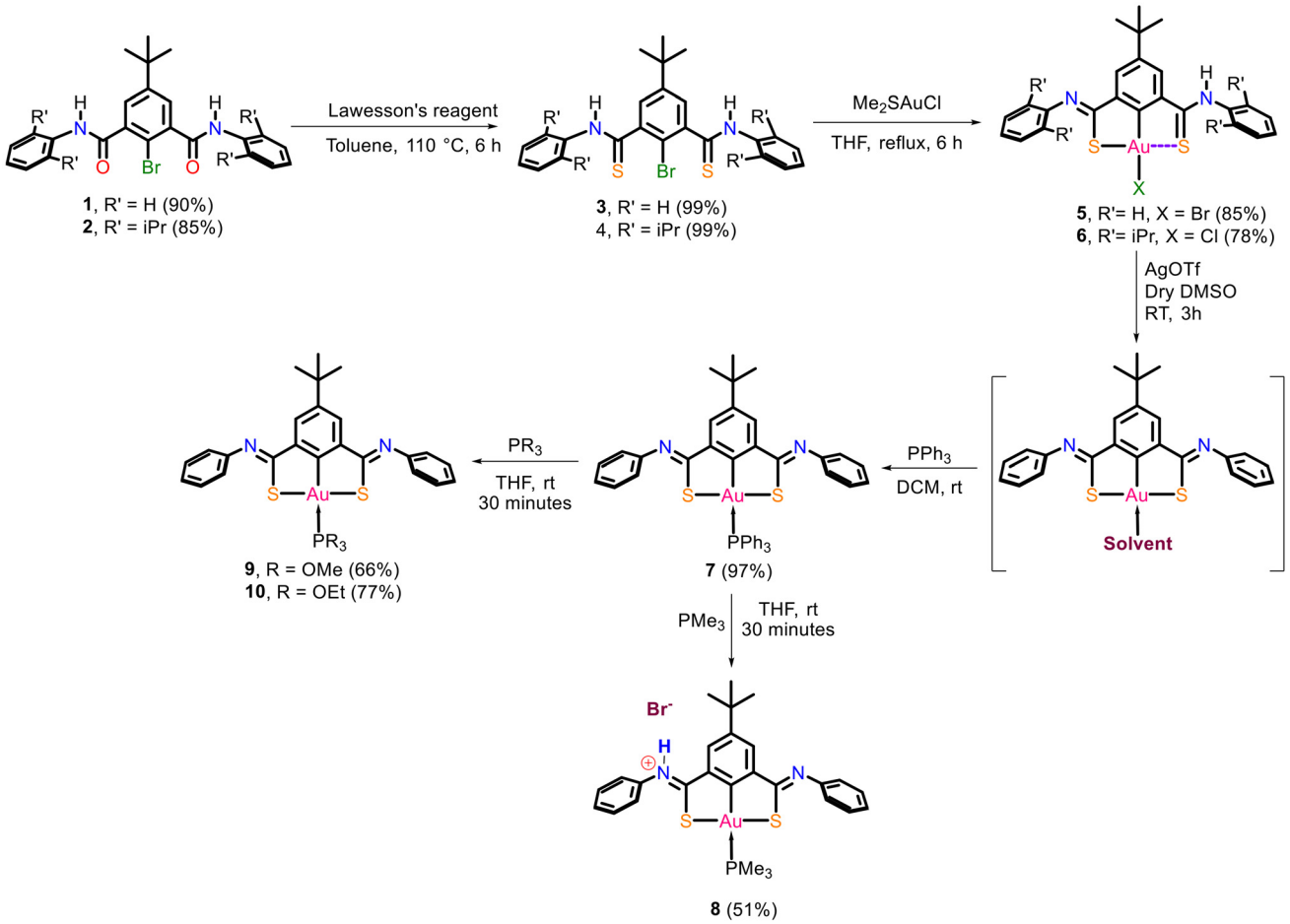

Scheme 2 Synthesis of SCS based Au(III) pincer complexes.

4 in nearly quantitative yields (99%).[76] The thioamide functionality is notable for its highly acidic proton, which upon deprotonation and *via* resonance forms the iminothiolate structure under mild basic conditions. These ligands act as multi-anionic donors depending on the charge of the coordinating metal ions.[77,78] Additionally, the sulfur atom in the thioamide group can both donate electrons to and accept electrons from the metal centre through its empty d-orbitals.[77,79] Given these properties, we aimed to isolate gold(III) complexes *via* oxidative addition of SCS pincer ligands to gold(I) precursors. The reaction of thio-iso-phthalamide **3** with the gold(I) precursor SMe_2AuCl resulted in oxidative addition of the C_{Ar}–Br bond, yielding the light-yellow gold(III) complex **5** in 85% yield (Scheme 2). However, complex **5** exhibited poor solubility in common solvents such as dichloromethane, chloroform, acetonitrile, DMF, and DMSO. To address the solubility issue, we synthesized the di-iso-propyl-substituted thio-iso-phthalamide ligand **4** and treated it with SMe_2AuCl, which resulted in a highly soluble gold(III) complex **6** in 78% yield.

In an attempt to synthesize cationic gold(III) complexes, we treated the gold(III) complex **5** with silver triflate, followed by the addition of triphenylphosphine (Scheme 2). Unexpectedly, this reaction led to the formation of the neutral gold(III) complex **7** in 97% yield *via* iminothiolate formation, converting the dianionic $SC^{(-)}S^{(-)}$ pincer ligand in **5** into a trianionic $S^{(-)}C^{(-)}S^{(-)}$ species (Fig. 1). This transformation was confirmed by ^{1}H NMR, FT-IR, and single-crystal X-ray diffraction analysis. Further derivatization of complex **7** led to the synthesis of complexes **8–10**, incorporating ancillary ligands such as trimethylphosphine, trimethyl, and triethyl phosphites, respectively. The significant diminish in the intensity of the N–H proton signal in the ^{1}H NMR spectra of complex **5**, relative to the free ligand, is consistent with partial deprotonation upon debromination (see SI, page S6, S26).[80] Similarly, the FT-IR spectra of **5** and **6** exhibited two distinct peaks at 1583/1554 cm^{-1} and

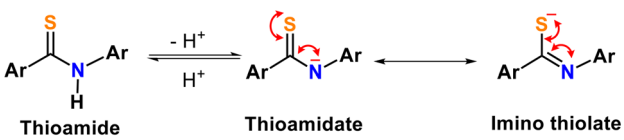

Fig. 1 Thioamide and possible resonance structures of its deprotonated thioamidate anion.

Table 1 Selected bond lengths (Å) and bond angles (°) of ligands **3**, **4**, and complexes **5–10**

	Ligands and Au(III) complexes							
Bond lengths (Å)/angles (°)	**3**	**4**	**5**	**6**	**7**	**8**	**9**	**10**
C1–Br1/Au1	1.892(2)	1.900(5)	1.992(6)	2.021(9), 2.001(10)	2.054(5)	2.037(9)	2.027(18)	2.024(4)
C11–S1	1.650(2)	1.652(5)	1.778(6)	1.794(9), 1.798(10)	1.805(6)	1.717(10)	1.784(2)	1.789(4)
C18–S2	1.662(3)	1.649(5)	1.720(6)	1.733(10), 1.712(10)	1.809(6)	1.783(9)	1.787(2)	1.783(4)
C11–N1	1.325(3)	1.328(6)	1.256(8)	1.269(12), 1.275(12)	1.269(7)	1.340(11)	1.280(3)	1.273(5)
C18–N2	1.336(3)	1.441(6)	1.319(8)	1.316(11), 1.314(11)	1.264(8)	1.276(12)	1.275(3)	1.277(6)
Au–Br1/Cl1/P1	—	—	2.432(9), 2.22(2)	2.490(3), 2.340(2) 2.430(2), 2.398(15)	2.385(15)	2.351(2)	2.334(5)	2.333(11)
Au1–S1	—	—	2.2871(16)	2.298(3), 2.298(3)	2.328(16)	2.317(3)	2.3176(5)	2.314(12)
Au1–S2	—	—	2.3193(16)	2.328(3), 2.340(3)	2.312(17)	2.292(3)	2.3156(5)	2.309(12)
C1–Au1–Br1/Cl1/P1	—	—	176.1(2), 173.9(8)	175.7(7), 178.5(7) 174.9(5), 176.1(4)	173.3(2)	176.7(3)	177.59(5)	176.7(1)
S1–Au1–S2	—	—	171.80(6)	171.71(10), 171.68(9)	170.34(6)	170.9(1)	170.72(2)	170.75(4)

1586/1552 cm^{-1}, corresponding to C=S and C–S stretching. In contrast, complexes **7–10** exhibited a single peak at 1583, 1604, 1580, and 1579 cm^{-1}, respectively, indicating iminothiolate (–N=C–S) formation.

The high-resolution mass spectra (HR-MS) of complexes **5** and **6** display a stable isotopic pattern with the corresponding (M + H) *m*/*z* values of 679.0148 and 847.2029, which suggest that the complexes **5** and **6** are formed by the deprotonation of the thio-iso-phthalamide ligand. Similarly, complexes **7–10** showed their discrete molecular ion peaks with *m*/*z* values at 861.14791 (M+), 675.1326 (M+), 723.1179 (M+), and 787.1460 (M + Na), respectively (see the SI).

Single crystal X-ray studies

For the X-ray diffraction analysis, suitable single crystals of **3**, **5**, and **6** were collected from NMR tubes by the slow evaporation of DMSO. Ligand **4** and complexes **7–10** were crystallized from chloroform (the crystal structures of ligands **3** and **4** are presented in the SI, page S60, Fig. S45, CCDC 2303816–2303823 for **3–10**, respectively). Complexes **5** and **6** crystallize in the monoclinic space groups $P2_1/c$ and $P2_1$, respectively. Both were isolated as yellow needle-shaped crystals, co-crystallized with DMSO, which engages in strong hydrogen bonding interactions with the thioamide N–H protons.

During oxidative addition of the C–Br bonds to SMe_2AuCl, halogen scrambling was observed, resulting in partially occupied halide sites: 0.28/0.72 (Cl/Br) in complex **5** and 0.77/0.23 and 0.75/0.25 (Cl/Br) in complex **6**, with both halogens coordinated to the gold centre.

Coordination to gold significantly induces planarization of the ligand backbone, as evidenced by the small dihedral angles between the central phenyl ring and the thioamide arms: 4.76(9)° and 3.13(17)° for **5**, and 3.5(7)°/4.8(8)° and 7.3 (7)°/2.5(7)° for the two independent molecules in **6**. Most importantly, the thio-iso-phthalamide ligands **3** and **4** act as dianionic species in complexes **5** and **6**; the changes in structural parameters and bond lengths strongly support that one thioamide arm in each complex (**5** and **6**) undergoes deprotonation followed by resonance forming an iminothiolate. The formation of the iminothiolate is evident from an increase in the C11=S1 bond length from 1.650(2) Å in the free ligand to 1.778(6) Å /1.788(10) Å in the complexes, accompanied by a decrease in the C–NH bond length from 1.449(7) Å to 1.258 (13)/1.254(12) Å (see Table 1). This transformation facilitates the oxidative addition of Au(I) to Au(III) and results in the formation of stable five-membered metallacycles (see Fig. 2).[78–80] On the other hand, the lengths of the resulting new Au–S bonds are unequal, due to uneven electron donation to the Au (III) center. In complex **5**, the length of the Au–S1 bond is 2.2908(15) Å, whereas for Au–S2 it is 2.3210(14) Å. Similarly, in complex **6** (Fig. 3), the Au–S1 distances are 2.293(3)/2.324(3) Å, while the Au–S2 distances are 2.337(3)/2.294(3) Å. These disparities clearly indicate the coexistence of both thiolato-like and thione-like binding modes within a single molecule, which is a characteristic consequence of the resonance in the coordinated thioamide ligands. Therefore, it suggests that the thioamide groups are converted into the iminothiolate form *via* resonance to facilitate the oxidative addition of a C–Br bond resulting in Au(III) complexes. Furthermore, the replacement of halide ions in complex **5** with neutral phosphine ligands led to the deprotonation of the second thioamide arm,

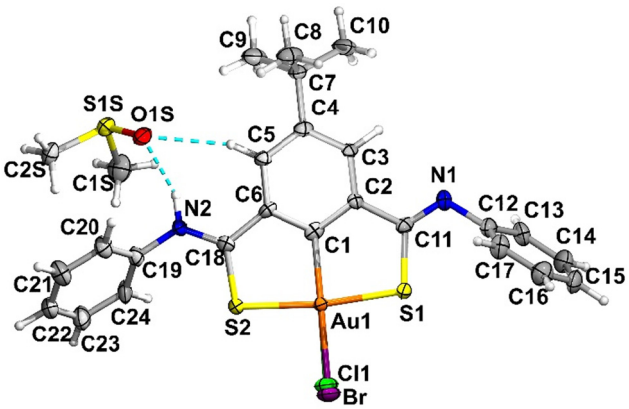

Fig. 2 Molecular structure of $S^{(-)}C^{(-)}S$ gold(III) complex **5** with 50% thermal ellipsoid probability.

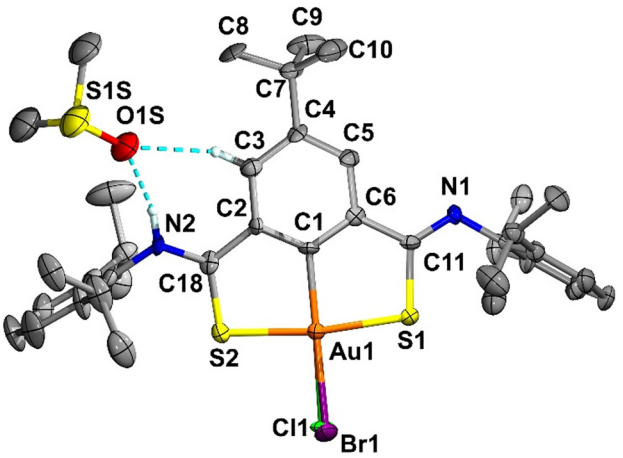

Fig. 3 Molecular structure of $S^{(-)}C^{(-)}S$ gold(III) complex **6** with 50% thermal ellipsoid probability. The unit cell contains two molecules; for clarity, hydrogen atoms, disordered atoms and one of the molecules are omitted.

resulting in the conversion of the trianionic $S^{(-)}C^{(-)}S^{(-)}$ pincer ligand, which led to coordinatively saturated neutral Au(III) complexes **7**, **8**, **9**, and **10** (Fig. 4). However, in complex **8**, one of the imine nitrogen atoms is protonated, forming an HBr salt that contains both thione and thiolato sulfur functionalities. The bromide ion is co-crystallized and participates in hydrogen bonding with the imine-H proton (Fig. 4).

In complexes **7**–**10**, both thioamide arms are deprotonated, forming bidentate thiolato coordination. Structural evidence includes elongated C11–S1 bonds (1.783–1.805 Å) and shortened C11═N1 bonds [*e.g.*, 1.280(3) Å in **7**, 1.264(8) Å in **6**].

In **8**, the two arms show different characters: S1 resembles thiolato, with longer C18–S2 and C–N1 = 1.340(11) Å, whereas S2 remains thione-like with C18–N2 = 1.276(12) Å.

All complexes **5**–**10** feature square planar Au(III) centers. The two sulfur donors define nearly linear S–Au–S angles ranging from 171.80(8)° to 173.69(6)°, while the C1–Au–X angles (X = Br, Cl, or P) fall between 173.3(2)° and 178.3(6)°. These orthogonal coordination axes result in $\sum$Au$\alpha \approx 351°$ and τ_4 values of 0.7–0.9, confirming a distorted square planar geometry. Notably, the S–Au–S angles observed here are broader than those typically reported for related Ni, Pd, and Pt complexes bearing similar d^8 electronic configurations (165.96°–175.20°).[76,81–88] This difference is attributed to the strong trianionic nature of the $S^{(-)}C^{(-)}S^{(-)}$ pincer ligands in **7**–**10**, which increases steric and electronic repulsion at the Au (III) center. Taken together, these observations demonstrate the remarkable flexibility of thio-iso-phthalamide-based carbophilic pincer ligands, which can function as monoanionic $SC^{(-)}S$, dianionic $SC^{(-)}S^{(-)}$, or trianionic $S^{(-)}C^{(-)}S^{(-)}$ donors depending on the coordination environment. Moreover, their adaptive donor behavior and strong electronic influence can effectively facilitate oxidative addition processes, expanding their potential utility in transition-metal-mediated transformations.

Cyclic voltammetry studies

The electrochemical behaviour of the ligands and their corresponding gold complexes was investigated by cyclic voltammetry (CV) at a scan rate of 100 mV s^{-1} within a potential window of −1.6 to +1.5 V.[89–92]

$$Au^{3+} \underset{Ox}{\overset{Red}{\rightleftharpoons}}_{2e^-} Au^{1+} \underset{Ox}{\overset{Red}{\rightleftharpoons}}_{1e^-} Au^0 \quad (1)$$

The electrochemical data indicate that the gold complexes exhibit a combination of quasi-reversible and irreversible redox behaviour, while the ligands **3** and **4** are electrochemically inactive within the potential range of −1.6 to +1.5 V (Table 2, Fig. 5, eqn (1)). However, complexes **5** and **6** display two cathodic peaks corresponding to sequential reductions of the gold(III) complex. The first reduction step, attributed to the Au(III) → Au(I) redox couple, occurs around 0.15–0.174 V with ΔE_p values of 138 mV for complex **5** and 100 mV for complex **6**, indicating quasi-reversible electron transfer. The second cathodic peak, corresponding to the Au(I) → Au(0) process, appears at −0.89 V for complex **5** and at −1.03 V for complex **6**, with ΔE_p values of 24 mV and 200 mV, respectively. Despite the relatively small ΔE_p for complex **5**, the absence of a corresponding anodic peak and the observation of gold deposition suggest that this process is electrochemically irreversible in both cases. Upon reversing the scan direction, weak anodic responses are detected at −0.65 V (for **5**) and −0.83 V (for **6**) ($Au^0 \rightarrow Au^+$), followed by additional oxidation peaks at 0.28 V (for **5**) and 0.27 V (for **6**) ($Au^+ \rightarrow Au^{3+}$), consistent with partial re-oxidation of the deposited elemental gold. These electrochemical characteristics align with literature reports on cyclometalated Au(III) complexes, which typically show cathodic reduction potentials in the range of −0.60 to −1.83 V.[92–95]

Similarly complexes **7**–**9** exhibit (Fig. S56) improved electrochemical characteristics. Complex **7** exhibits an Au(III)/Au(I) couple at −0.015/+0.026 V with a ΔE_p of 41 mV, approaching the ideal value for a reversible one-electron process. Complexes **8** and **9** also show similar behavior with ΔE_p values of 50 mV and 20 mV, respectively, indicating that the electron transfer kinetics are fast and the Au(III)/Au(I) processes are effectively reversible. However, the Au(I)/Au(0) redox processes in these complexes are characterized by significantly larger ΔE_p values (300 mV for **7**, 200 mV for **8**, and 150 mV for **9**), confirming that these reductions are electrochemically irreversible, likely due to the instability of the Au(0) state and the associated deposition on the electrode surface. In contrast, complex **10** exhibits distorted electrochemical behavior with large ΔE_p values for both the Au (III)/Au(I) (−0.29/+0.38 V, ΔE_p = 670 mV) and Au(I)/Au(0) (−1.23/−0.27 V, ΔE_p = 960 mV) couples. Such large peak separations indicate that both redox processes are irreversible, likely due to severe structural rearrangements, sluggish electron transfer kinetics, or unstable redox intermediates. Collectively, these results confirm that all observed redox events are metal-centered, as the ligands are redox-inactive. The Au(III)/Au(I) couple ranges from quasi-reversible (complexes **5** and **6**) to reversible (complexes **7**–**9**), while the Au(I)/Au(0) couple is consistently irre-

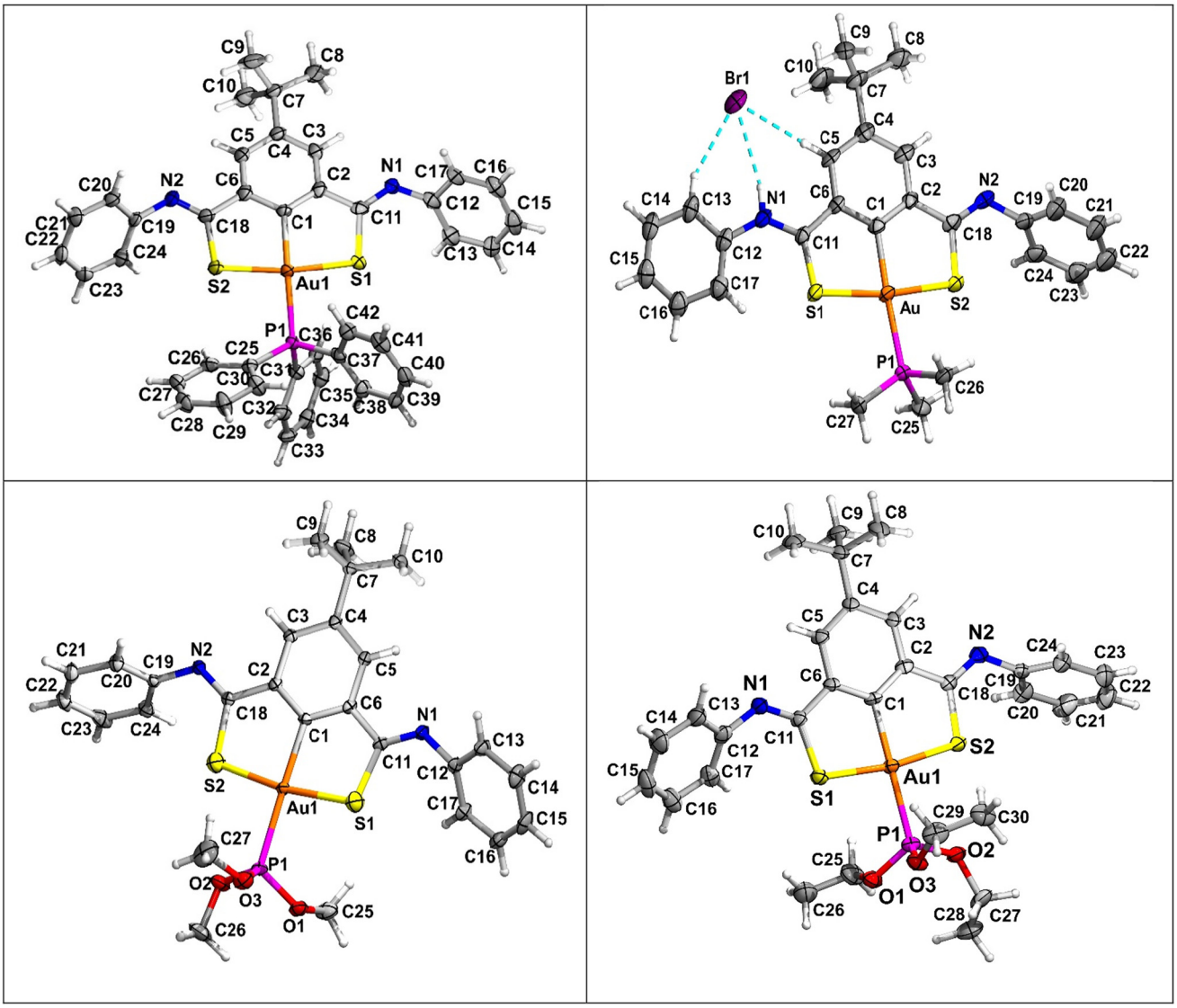

Fig. 4 Molecular structure of complex **7** (above left), complex **8** (above right), complex **9** (below left), and complex **10** (below right), with 50% thermal ellipsoid probability.

versible across all complexes, primarily due to the reduction to elemental gold and the difficulty of re-oxidizing Au(0) under the experimental conditions.

These irreversible redox profiles indicate that the gold ion predominantly exists in the +3-oxidation state in all thio-iso-phthalamide pincer gold complexes (**5–10**), while the corresponding reduced species (Au(I) and Au(0)) are unstable under the applied electrochemical conditions. Moreover, the Au(I)/Au(0) redox couple occurring at more negative potentials suggests that the gold centre is situated in a highly stabilizing ligand environment, which further resists reduction and reinforces the thermodynamic preference for the Au(III) oxidation state.

Computational studies

The coordination modes of tridentate thio-iso-phthalamide ligands with transition metal ions have been reported only for a limited number of complexes,[80] and mechanistic insights into their reactivity remain largely unexplored at the computational level. To elucidate the mechanism underlying the formation of the gold(III) complex **5**, we carried out gas-phase density functional theory (DFT) calculations at the B3PW91 level of theory, employing the SDD basis set for gold and the 6-311+G(d,p) basis set for H, C, N, S, Cl, and Br atoms, using the Gaussian09 software package.[96] Inspired by the potential influence of the two thioamide donor arms on the oxidative addition of the C_{Ar}–Br bond, we examined the reaction pathway leading to complex **5**. The calculations indicate that bidentate coordination involving both thioamide sulphur donors, as represented in intermediate $\mathbf{I_b}$, precedes a kinetically feasible oxidative addition of the C_{Ar}–Br bond to the gold centre, with an associated free energy of activation ($\Delta G^{\ddagger}$) of 25.2 kcal mol^{-1} (Fig. 6).[68,97] For comparison, in the

Table 2 The oxidation and reduction potential of ligands and Au(III) complexes **3–10**

Ligand and complex	First redox couple, Au(III)/Au(I) (V)	Second redox couple, Au(I)/Au(0) (V)	ΔE_p (mV)
3	NO	NO	—
4	NO	NO	—
5	+0.15, +0.28	−0.89, −0.65	138; 24
6	+0.17, +0.27	−1.03, −0.83	100; 200
7	−0.015, +0.026	−1.24, −0.94	41; 300
8	+0.17, +0.22	−0.94, −1.14	50; 200
9	+0.12, +0.14	−1.22, −1.07	20; 150
10	−0.29, +0.38	−1.23, −0.27	670; 960

NO = not observed.

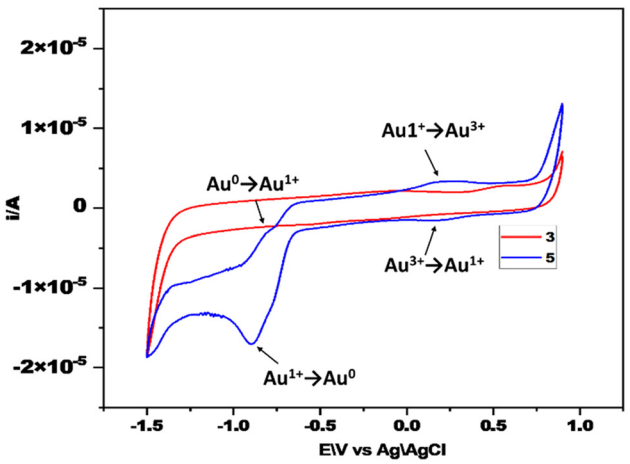

Fig. 5 Cyclic voltammograms of ligand **3** and complex **5** in 1 mM DMSO solution at a scan rate of 100 mV s^{-1} with 0.1 M $(n\text{-Bu})_4PF_6$ as the supporting electrolyte.

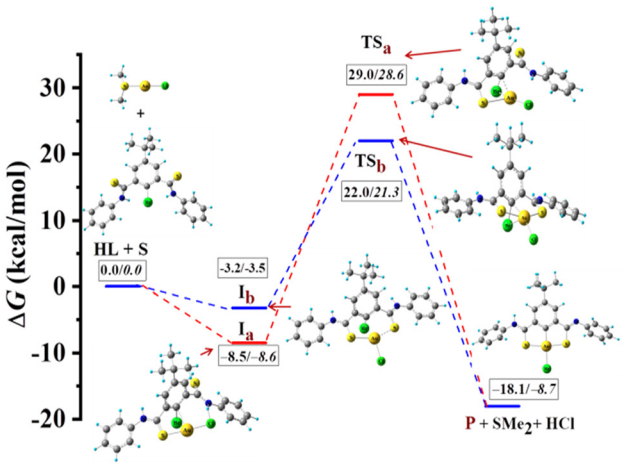

Fig. 6 Gibbs free energy profile computed at the B3PW91/SDD (Au), 6-311+g** (H, C, N, S, Cl, and Br) level of theory for the oxidative addition of the C_{Ar}–Br bond. $\Delta G^{\ddagger}/\Delta H^{\ddagger}$ values are given in kcal mol^{-1}.

diphosphine-based system reported by Bourissou *et al.*, the computed transition state energy is slightly lower.[68] The relatively high activation barrier in our case may be attributed to the stronger coordination ability of the sulphur donors or possibly the involvement of an iminothiolate-type resonance structure that affects the ligand's electronic properties. Alternatively, a monodentate coordination pathway (intermediate $\mathbf{I_a}$) was also evaluated, wherein only one thioamide arm interacts with the gold(I) center. Although $\mathbf{I_a}$ is thermodynamically more stable than the bidentate complex $\mathbf{I_b}$ by 5.3 kcal mol^{-1}, the oxidative addition barrier is substantially higher with $\Delta G^{\ddagger}$ = 37.5 kcal mol^{-1}, making this pathway kinetically unfavorable.

These computational results underscore the critical role of the second thioamide donor arm in facilitating the oxidative addition step. The chelation effect stabilizes the transition state and effectively lowers the activation energy barrier, thereby promoting the efficient formation of the gold(III) complex **5**. The tridentate thio-iso-phthalamide ligand framework thus provides an enhanced coordination environment around the gold(I) center, increasing its reactivity toward oxidative addition.

In vitro cytotoxicity studies

In complexes **5** and **7–10**, the gold centre is in the +3 oxidation state, which is isoelectronic (d^8) with Pt(II) and with coordination sites $S^{(-)}C^{(-)}S^{(-)}$ mimicking the four coordinated *cis*-platin drug. Also, the reduction potentials [Au^{III} to Au^{I} to Au^{0} = −0.89 to −1.23 V] of the complexes **7–10** are more negative than the reported redox potential of glutathione (−0.36 V).[98] This suggests that it may not be possible to reduce Au^{I} into Au^{0} in the synthesized complexes **5** and **7–10** by thiol in a biological system. Furthermore, the neutral ancillary ligands in the synthesized gold(III) complexes can undergo exchange with the neutral ligands from the biological system.[99–109] Also, recent reports suggest that organogold complexes exhibit potent anticancer activities with improved selectivity.[110,111] Motivated by these findings, we evaluated the *in vitro* cytotoxicity of the synthesized ligand **3** and Au(III) complexes **5** and **7–10** against the cancerous MDA-MB-231 (M.D. Anderson-Metastatic Breast 231) cells and non-cancerous L929 (NCTC clone) cell lines (Table 3 and Fig. 7). The inhibition of the pro-

Table 3 The IC_{50} values (μM) for the ligand and Au(III) complexes

Entry	Ligand/Au(III) complexes	IC_{50} (μM) for non-cancerous L929 cells	IC_{50} (μM) for cancerous MDA-MB-231 cells
1	Ligand **3**	>75	75
2	**Au(III)–Br complex 5**	**30**	**15**
3	Au(III)–PPh_3 complex **7**	75	60
4	Au(III)–PMe_3 complex **8**	30	30
5	**Au(III)–$P(OMe)_3$ complex 9**	**>75**	**30**
6	Au(III)–$P(OEt)_3$ complex **10**	60	45

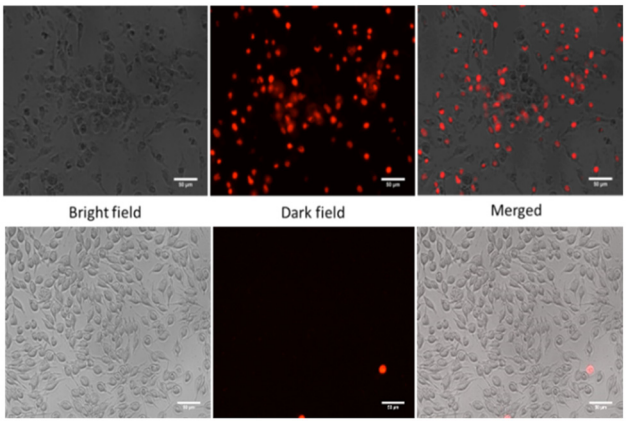

Fig. 7 Fluorescence microscopic images of cancerous MDA-MB-231 cells (top) and non-cancerous **L929** cells (down) that have undergone apoptosis, stained with PI for the Au(III)–$P(OMe)_3$ complex **9** at a concentration of 45 μM. In the left – bright field image, in the middle – dark field image, and in the right – merged image.

liferation of these cell lines was determined using the established MTT assay (for experimental details please see SI Fig. S71 and S72, page S93–S94).

The observations made with both the cancerous and non-cancerous cells are presented in Table 3 (see SI Fig. S71 and S72). It is noticed that the Au(III)–Br complex **5** exhibits promising cytotoxicity in the case of both cancerous MDA-MB-231 cells and non-cancerous L929 cells (Table 3, entry 2). Very interestingly, the trimethoxy phosphite-ligated Au(III) complex **9** exhibits excellent and targeted cytotoxicity towards cancerous cells even at low concentrations, while having a minimal effect on normal non-cancerous cells even at higher concentrations (Table 3, entry 5).

To identify the dead cells, propidium iodide (PI) was used for staining the cells which were in the apoptotic phase. In accordance with *in vitro* cytotoxicity studies (Table 3), we observed least PI staining in both cancerous MDA-MB-231 and non-cancerous L929 cells in the presence of ligand **3** and Au(III)–PPh_3 complex **7** (see the red spots in SI Fig. S73 and S74, page S96–S97), indicating their least suitability as anticancer agents. The staining with the Au(III)–$P(OEt)_3$ complex **10** is moderate. Notably, the number of both the cancerous MDA-MB-231 and non-cancerous L929 cells, stained with PI, was very high in the cases of Au(III)–Br complex **5** and Au(III)–PMe_3 complex **8**. This suggested the high cytotoxicity of both the complexes **5** and **8**, as most of the cells (both cancerous and non-cancerous) entered the apoptotic phase (see the red spots in SI Fig. S73 and S74).

To our delight, in the presence of the Au(III)–$P(OMe)_3$ complex **9**, a large number of cancerous MDA-MB-231 cells were stained with PI, but only a few non-cancerous cells were stained (Fig. 7). This highlights the fascinating behaviour of the complex **9** for 'targeted therapy' as it can selectively kill the cancerous cells, while keeping the normal cells unaffected.

Conclusion

In summary, we successfully synthesized and characterized pincer gold(III) complexes using thio-iso-phthalamide pincer ligands by the oxidative addition of aryl $C(sp^2)$–Br bonds to the Au(I) centre, which have been underexplored to date. Furthermore, we have synthesized a highly stable, neutral, carbophilic thioamide organogold(III) complex for the first time. It is important to note that the thio-iso-phthalamide pincer ligands act as monoanionic $SC^{(-)}S$ and dianionic $SC^{(-)}S^{(-)}$ type pincer ligands with Ni, Pd, and Pt metals; whereas in gold(III) chemistry, thio-iso-phthalamide serves as a $S^{(-)}C^{(-)}S^{(-)}$ trianionic ligand. The synthesized thio-iso-phthalamide ligands exhibited iminothiolate resonance, enhancing their coordination ability and stabilizing gold(III) complexes. Spectroscopic and X-ray analyses confirmed ligand deprotonation, iminothiolate formation, and a square planar geometry with strong Au–S bonds. Cyclic voltammetry revealed irreversible Au(III) → Au(I) → Au(0) redox behavior, with reduction peaks at more negative potentials indicating enhanced stability. Computational studies showed that bidentate chelation reduced the oxidative addition barrier, while Wiberg bond order, AIM, and NAO analyses confirmed stronger Au–S bonding and electron delocalization, reinforcing complex stability. Moreover, the synthesized gold complex **5** demonstrated high anticancer activity, while gold complex **9** exhibited selective toxicity toward cancer cells even at low concentrations, highlighting its potential for targeted therapy.

Overall, this study highlights the use of thio-iso-phthalamide ligands as an effective strategy for the oxidative addition of the C_{Ar}–Br bond to Au(I) to afford stable gold(III) complexes, offering valuable insights for designing stable Au-based molecules. Also, the remarkable selective toxicity of the synthesized gold complex towards cancerous cells opens new avenues for further studies on 'targeted cancer therapy'. Further investigations on the catalytic activity of these $S^{(-)}C^{(-)}S^{(-)}$-Au(III)PR_3 complexes are currently under progress.

Author contributions

The manuscript was written through the contributions of all authors. All authors have given approval to the final version of the manuscript.

Conflicts of interest

No conflicts of interest.

Data availability

For detailed synthetic procedures, data characterization, X-ray diffraction structural analyses, and geometries and energies of theoretically investigated structures. see DOI: **https://doi.org/10.1039/d5dt00916b**.

CCDC 2303816–2303823 contain the supplementary crystallographic data for this paper.[112a–h]

Acknowledgements

H. B. S. and S. K. sincerely acknowledge DST-SERB, J. C. Bose Fellowship 15DSTFLS002, Grant No. RD/0115-DSTFLS80-004, CSIR New Delhi and IIT Bombay for the infrastructure and financial support. S. K. would like to thank ANRF-SERB (CRG/2023/002473) New Delhi and IISER Bhopal for financial support. S. R. sincerely acknowledges IISER Bhopal for a post-doctoral fellowship. S. S. acknowledges DST-INSPIRE (IF170996) for a fellowship.

References

1 M. N. Hopkinson, A. Tlahuext-Aca and F. Glorius, *Acc. Chem. Res.*, 2016, **49**, 2261–2272.
2 D. J. Gorin and F. D. Toste, *Nature*, 2007, **446**, 395–403.
3 D. J. Gorin, B. D. Sherry and F. D. Toste, *Chem. Rev.*, 2008, **108**, 3351–3378.
4 M. Rigoulet, O. Thillaye du Boullay, A. Amgoune and D. Bourissou, *Angew. Chem., Int. Ed.*, 2020, **59**, 16625–16630.
5 C. C. Chintawar, V. W. Bhoyare, M. V. Mane and N. T. Patil, *J. Am. Chem. Soc.*, 2022, **144**, 7089–7095.
6 S. P. Sancheti, Y. Singh, M. V. Mane and N. T. Patil, *Angew. Chem., Int. Ed.*, 2023, **62**, e202310493.
7 V. W. Bhoyare, E. D. Sosa Carrizo, C. C. Chintawar, V. Gandon and N. T. Patil, *J. Am. Chem. Soc.*, 2023, **145**, 8810–8816.
8 D. M. Grove, G. van Koten and R. Zoet, *J. Am. Chem. Soc.*, 1983, **105**, 1379–1380.
9 D. M. Grove, G. van Koten, P. Mul, R. Zoet, J. G. M. van der Linden, J. Legters, J. E. J. Schmitz, N. W. Murrall and A. J. Welch, *Inorg. Chem.*, 1988, **27**, 2466–2473.
10 M. Contel, D. Nobel, A. L. Spek and G. van Koten, *Organometallics*, 2000, **19**, 3288–3295.
11 M. Contel, M. Stol, M. A. Casado, G. P. M. van Klink, D. D. Ellis, A. L. Spek and G. van Koten, *Organometallics*, 2002, **21**, 4556–4559.
12 B. F. Straub, *Angew. Chem., Int. Ed.*, 2010, **49**, 7622–7622.
13 Y. Yang, L. Eberle, F. F. Mulks, J. F. Wunsch, M. Zimmer, F. Rominger, M. Rudolph and A. S. K. Hashmi, *J. Am. Chem. Soc.*, 2019, **141**, 17414–17420.
14 M. A. Carvajal, J. J. Novoa and S. Alvarez, *J. Am. Chem. Soc.*, 2004, **126**, 1465–1477.
15 T. J. O'Connor and F. D. Toste, *ACS Catal.*, 2018, **8**, 5947–5951.
16 P. T. Bohan and F. D. Toste, *J. Am. Chem. Soc.*, 2017, **139**, 11016–11019.
17 C.-Y. Wu, T. Horibe, C. B. Jacobsen and F. D. Toste, *Nature*, 2015, **517**, 449–454.
18 X.-z. Shu, M. Zhang, Y. He, H. Frei and F. D. Toste, *J. Am. Chem. Soc.*, 2014, **136**, 5844–5847.
19 M. W. Johnson, A. G. DiPasquale, R. G. Bergman and F. D. Toste, *Organometallics*, 2014, **33**, 4169–4172.
20 W. Zi and F. D. Toste, *J. Am. Chem. Soc.*, 2013, **135**, 12600–12603.
21 S. G. Sethofer, T. Mayer and F. D. Toste, *J. Am. Chem. Soc.*, 2010, **132**, 8276–8277.
22 N. D. Shapiro and F. D. Toste, *J. Am. Chem. Soc.*, 2007, **129**, 4160–4161.
23 Y. Horino, M. R. Luzung and F. D. Toste, *J. Am. Chem. Soc.*, 2006, **128**, 11364–11365.
24 B. D. Sherry and F. D. Toste, *J. Am. Chem. Soc.*, 2004, **126**, 15978–15979.
25 H. A. Wegner and M. Auzias, *Angew. Chem., Int. Ed.*, 2011, **50**, 8236–8247.
26 T. C. Boorman and I. Larrosa, *Chem. Soc. Rev.*, 2011, **40**, 1910–1925.
27 B. Sahoo, M. N. Hopkinson and F. Glorius, *J. Am. Chem. Soc.*, 2013, **135**, 5505–5508.
28 P. Gualco, S. Ladeira, K. Miqueu, A. Amgoune and D. Bourissou, *Angew. Chem., Int. Ed.*, 2011, **50**, 8320–8324.
29 P. Gualco, S. Ladeira, K. Miqueu, A. Amgoune and D. Bourissou, *Organometallics*, 2012, **31**, 6001–6004.
30 M. Joost, P. Gualco, Y. Coppel, K. Miqueu, C. E. Kefalidis, L. Maron, A. Amgoune and D. Bourissou, *Angew. Chem., Int. Ed.*, 2014, **53**, 747–751.
31 N. Lassauque, P. Gualco, S. Mallet-Ladeira, K. Miqueu, A. Amgoune and D. Bourissou, *J. Am. Chem. Soc.*, 2013, **135**, 13827–13834.
32 M. Joost, A. Amgoune and D. Bourissou, *Angew. Chem., Int. Ed.*, 2015, **54**, 15022–15045.
33 J. Serra, C. J. Whiteoak, F. Acuña-Parés, M. Font, J. M. Luis, J. Lloret-Fillol and X. Ribas, *J. Am. Chem. Soc.*, 2015, **137**, 13389–13397.
34 M. J. Harper, C. J. Arthur, J. Crosby, E. J. Emmett, R. L. Falconer, A. J. Fensham-Smith, P. J. Gates, T. Leman, J. E. McGrady, J. F. Bower and C. A. Russell, *J. Am. Chem. Soc.*, 2018, **140**, 4440–4445.
35 Y. Yang, P. Antoni, M. Zimmer, K. Sekine, F. F. Mulks, L. Hu, L. Zhang, M. Rudolph, F. Rominger and A. S. K. Hashmi, *Angew. Chem., Int. Ed.*, 2019, **58**, 5129–5133.
36 M. Navarro, A. Toledo, M. Joost, A. Amgoune, S. Mallet-Ladeira and D. Bourissou, *Chem. Commun.*, 2019, **55**, 7974–7977.
37 A. Tamaki and J. K. Kochi, *J. Organomet. Chem.*, 1972, **40**, C81–C84.
38 A. Shiotani and H. Schmidbaur, *J. Organomet. Chem.*, 1972, **37**, C24–C26.
39 A. Johnson and R. J. Puddephatt, *Inorg. Nucl. Chem. Lett.*, 1973, **9**, 1175–1177.
40 D. Eppel, P. Penert, J. Stemmer, C. Bauer, M. Rudolph, M. Brückner, F. Rominger and A. S. K. Hashmi, *Chem. – Eur. J.*, 2021, **27**, 8673–8677.

41 D. Eppel, M. Rudolph, F. Rominger and A. S. K. Hashmi, *ChemSusChem*, 2020, **13**, 1986–1990.
42 L. Huang, F. Rominger, M. Rudolpha and A. S. K. Hashmi, *Chem. Commun.*, 2016, **52**, 6435–6438.
43 L. Huang, M. Rudolph, F. Rominger and A. S. K. Hashmi, *Angew. Chem., Int. Ed.*, 2016, **55**, 4808–4813.
44 C. González-Arellano, A. Abad, A. Corma, H. García, M. Iglesias and F. Sánchez, *Angew. Chem., Int. Ed.*, 2007, **46**, 1536–1538.
45 S. Sasmal, M. Debnath, S. K. Nandi and D. Haldar, *Nanoscale Adv.*, 2019, **1**, 1380–1386.
46 P. S. D. Robinson, G. N. Khairallah, G. da Silva, H. Lioe and R. A. J. O'Hair, *Angew. Chem., Int. Ed.*, 2012, **51**, 3812–3817.
47 G. van Koten, *Pure Appl. Chem.*, 1989, **61**, 1681–1694.
48 M. Stol, D. J. M. Snelders, H. Kooijman, A. L. Spek, G. P. M. van Klinka and G. van Koten, *Dalton Trans.*, 2007, 2589–2593.
49 M. Robitzer, I. Bouamaïed, C. Sirlin, P. A. Chase, G. van Koten and M. Pfeffer, *Organometallics*, 2005, **24**, 1756–1761.
50 G. van Koten, *Organometallic pincer chemistry*, Springer, 2013; pp 1–20.
51 P. A. Chase, R. A. Gossage and G. van Koten, *Top. Organomet. Chem.*, 2016, **54**, 1–15.
52 G. van Koten, *J. Organomet. Chem.*, 2013, **730**, 156–164.
53 G. van Koten and D. Milstein, *Organometallic pincer chemistry*, Springer, 2012.
54 G. van Koten, *Top. Organomet. Chem.*, 2013, **40**, 1–20.
55 D. Zargarian, A. Castonguay and D. M. Spasyuk, in *Organometallic Pincer Chemistry*, ed. G. van Koten and D. Milstein, Springer Berlin Heidelberg, Berlin, Heidelberg, 2013, pp. 131–173.
56 D. M. Grove, G. van Koten, P. Mul, R. Zoet, J. G. M. Van der Linden, J. Legters, J. E. J. Schmitz, N. W. Murrall and A. J. Welch, *Inorg. Chem.*, 1988, **27**, 2466–2473.
57 D. M. Grove, G. van Koten, R. Zoet, N. W. Murrall and A. J. Welch, *J. Am. Chem. Soc.*, 1983, **105**, 1379–1380.
58 D. M. Grove, G. van Koten and A. H. M. Verschuuren, *J. Mol. Catal.*, 1988, **45**, 169–174.
59 D. M. Grove, A. H. M. Verschuuren, G. van Koten and J. A. M. van Beek, *J. Organomet. Chem.*, 1989, **372**, C1–C6.
60 L. A. van de Kuil, D. M. Grove, R. A. Gossage, J. W. Zwikker, L. W. Jenneskens, W. Drenth and G. van Koten, *Organometallics*, 1997, **16**, 4985–4994.
61 R. A. Gossage, L. A. van de Kuil and G. van Koten, *Acc. Chem. Res.*, 1998, **31**, 423–431.
62 R. A. Gossage and G. van Koten, in *Activation of Unreactive Bonds and Organic Synthesis*, ed. S. Murai, H. Alper, R. A. Gossage, V. V. Grushin, M. Hidai, Y. Ito, W. D. Jones, F. Kakiuchi, G. van Koten, Y. S. Lin, Y. Mizobe, S. Murai, M. Murakami, T. G. Richmond, A. Sen, M. Suginome and A. Yamamoto, Springer Berlin Heidelberg, Berlin, Heidelberg, 1999, pp. 1–8.
63 G. van Koten, *J. Organomet. Chem.*, 2017, **845**, 4–18.
64 C. J. Moulton and B. L. Shaw, *J. Chem. Soc., Dalton Trans.*, 1976, 1020–1024.
65 G. van Koten, K. Timmer, J. G. Noltes and A. L. Spek, *J. Chem. Soc., Chem. Commun.*, 1978, 250–252.
66 H. Valdes, N. Alpuente, P. Salvador, A. S. K. Hashmi and X. Ribas, *Chem. Sci.*, 2024, **15**, 17618–17628.
67 F. Rekhroukh, R. Brousses, A. Amgoune and D. Bourissou, *Angew. Chem., Int. Ed.*, 2015, **54**, 1266–1269.
68 J. Guenther, S. Mallet-Ladeira, L. Estevez, K. Miqueu, A. Amgoune and D. Bourissou, *J. Am. Chem. Soc.*, 2014, **136**, 1778–1781.
69 M. Joost, A. Zeineddine, L. Estévez, S. Mallet-Ladeira, K. Miqueu, A. Amgoune and D. Bourissou, *J. Am. Chem. Soc.*, 2014, **136**, 14654–14657.
70 J. H. Teles, *Angew. Chem., Int. Ed.*, 2015, **54**, 5556–5558.
71 A. Ahrens, L. F. P. Karger, F. Rominger, M. Rudolph and A. S. K. Hashmi, *Organometallics*, 2023, **42**, 1561–1566.
72 J. Serra, T. Parella and X. Ribas, *Chem. Sci.*, 2017, **8**, 946–952.
73 V. Rani, H. B. Singh and R. J. Butcher, *Organometallics*, 2017, **36**, 4741–4752.
74 V. Rani, M. Boda, S. Raju, G. N. Patwari, H. B. Singh and R. J. Butcher, *Dalton Trans.*, 2018, **47**, 9114–9127.
75 S. S. Zade, S. Panda, S. K. Tripathi, H. B. Singh and G. Wolmershäuser, *Eur. J. Org. Chem.*, 2004, 3857–3864.
76 R. A. Begum, D. Powell and K. Bowman-James, *Inorg. Chem.*, 2006, **45**, 964–966.
77 K. Okamoto, J. Kuwabara and T. Kanbara, *Chem. Lett.*, 2014, **44**, 102–110.
78 J. V. Micallef and D. P. N. Satchell, *Inorg. Chim. Acta*, 1982, **64**, L187.
79 Y. Komiyama, J. Kuwabara and T. Kanbara, *Organometallics*, 2014, **33**, 885–891.
80 K. Okamoto, J. Kuwabara and T. Kanbara, *Chem. Lett.*, 2015, **44**, 102–110.
81 T.-a. Koizumi, T. Teratani, K. Okamoto, T. Yamamoto, Y. Shimoi and T. Kanbara, *Inorg. Chim. Acta*, 2010, **363**, 2474–2480.
82 T. Kanbara, K. Okada, T. Yamamoto, H. Ogawa and T. Inoue, *J. Organomet. Chem.*, 2004, **689**, 1860–1864.
83 K. Okamoto, T. Kanbara, T. Yamamoto and A. Wada, *Organometallics*, 2006, **25**, 4026–4029.
84 J. Kuwabara, G. Munezawa, K. Okamoto and T. Kanbara, *Dalton Trans.*, 2010, **39**, 6255–6261.
85 M. Akaiwa, T. Kanbara, H. Fukumoto and T. Yamamoto, *J. Organomet. Chem.*, 2005, **690**, 4192–4196.
86 J. Kuwabara, Y. Ogawa, A. Taketoshi and T. Kanbara, *J. Organomet. Chem.*, 2011, **696**, 1289–1293.
87 M. A. Hossain, S. Lucarini, D. Powell and K. Bowman-James, *Inorg. Chem.*, 2004, **43**, 7275–7277.
88 H. Honda, Y. Ogawa, J. Kuwabara and T. Kanbara, *Eur. J. Inorg. Chem.*, 2014, **2014**, 1865–1869.
89 N. Elgrishi, K. J. Rountree, B. D. McCarthy, E. S. Rountree, T. T. Eisenhart and J. L. Dempsey, *J. Chem. Educ.*, 2018, **95**, 197–206.
90 A. Maroń, K. Czerwińska, B. Machura, L. Raposo, C. Roma-Rodrigues, A. R. Fernandes, J. G. Małecki,

A. Szlapa-Kula, S. Kula and S. Krompiec, *Dalton Trans.*, 2018, **47**, 6444–6463.
91 M. D. Đurović, R. Puchta, Ž. D. Bugarčić and R. van Eldik, *Dalton Trans.*, 2014, **43**, 8620–8632.
92 H. V. Huynh, S. Guo and W. Wu, *Organometallics*, 2013, **32**, 4591–4600.
93 M. V. Babak, K. R. Chong, P. Rapta, M. Zannikou, H. M. Tang, L. Reichert, M. R. Chang, V. Kushnarev, P. Heffeter and S. M. Meier-Menches, *Angew. Chem., Int. Ed.*, 2021, **60**, 13405–13413.
94 S. Gukathasan, S. Parkin and S. G. Awuah, *Inorg. Chem.*, 2019, **58**, 9326–9340.
95 J. H. Kim, E. Reeder, S. Parkin and S. G. Awuah, *Sci. Rep.*, 2019, **9**, 12335.
96 M. J. Frisch, G. W. Trucks, H. B. Schlegel, G. E. Scuseria, M. A. Robb, J. R. Cheeseman, G. Scalmani, V. Barone, B. Mennucci, G. A. Petersson, H. Nakatsuji, M. Caricato, X. Li, H. P. Hratchian, A. F. Izmaylov, J. Bloino, G. Zheng, J. L. Sonnenberg, M. Hada, M. Ehara, K. Toyoto, R. Fukuda, J. Hasegawa, M. Ishida, T. Nakajima, Y. Honda, O. Kitao, H. Nakai, T. Vreven, J. A. Montgomery Jr., J. Peralta, F. Ogliaro, M. Bearpark, J. J. Heyd, E. Brothers, K. N. Kudin, V. N. Staroverov, R. Kobayashi, J. Normand, K. Raghavachari, A. Rendell, J. C. Burant, S. S. Iyengar, J. Tomasi, M. Cossi, N. Rega, J. M. Millam, M. Klene, J. E. Knox, J. B. Cross, V. Bakken, C. Adamo, J. Jaramillo, R. Gomperts, R. E. Stratmann, O. Yazyev, A. J. Austin, R. Cammi, C. Pomelli, J. W. Ochterski, R. L. Martin, K. Morokuma, V. G. Zakrzewski, G. A. Voth, P. Salvador, J. J. Dannenberg, S. Dapprich, A. D. Daniels, O. Farkas, J. B. Foresman, J. V. Ortiz, J. Cioslowski and D. J. Fox, *Gaussian 09, Revision A.02*, Gaussian, Inc., Wallingford CT, 2009.
97 C. Blons, S. Mallet-Ladeira, A. Amgoune and D. Bourissou, *Angew. Chem., Int. Ed.*, 2018, **57**, 11732–11736.
98 A. Mirzahosseini and B. Noszál, *Sci. Rep.*, 2016, **6**, 1–11.
99 G. Moreno-Alcántar, P. Picchetti and A. Casini, *Angew. Chem., Int. Ed.*, 2023, **62**, e202218000.
100 Y. Lu, X. Ma, X. Chang, Z. Liang, L. Lv, M. Shan, Q. Lu, Z. Wen, R. Gust and W. Liu, *Chem. Soc. Rev.*, 2022, **51**, 5518–5556.
101 J.-J. Zhang, M. A. Abu el Maaty, H. Hoffmeister, C. Schmidt, J. K. Muenzner, R. Schobert, S. Wölfl and I. Ott, *Angew. Chem., Int. Ed.*, 2020, **59**, 16795–16800.
102 V. Fernández-Moreira, R. P. Herrera and M. C. Gimeno, *Pure Appl. Chem.*, 2019, **91**, 247–269.
103 M. Fereidoonnezhad, H. R. Shahsavari, E. Lotfi, M. Babaghasabha, M. Fakhri, Z. Faghih, Z. Faghih and M. Hassan Beyzavi, *Appl. Organomet. Chem.*, 2018, **32**, e4200.
104 B. Bertrand, M. R. Williams and M. Bochmann, *Chem. – Eur. J.*, 2018, **24**, 11840–11851.
105 M. Negom Kouodom, L. Ronconi, M. Celegato, C. Nardon, L. Marchio, Q. P. Dou, D. Aldinucci, F. Formaggio and D. Fregona, *J. Med. Chem.*, 2012, **55**, 2212–2226.
106 A. Meyer, C. P. Bagowski, M. Kokoschka, M. Stefanopoulou, H. Alborzinia, S. Can, D. H. Vlecken, W. S. Sheldrick, S. Wölfl and I. Ott, *Angew. Chem., Int. Ed.*, 2012, **51**, 8895–8899.
107 S. D. Köster, H. Alborzinia, S. Can, I. Kitanovic, S. Wölfl, R. Rubbiani, I. Ott, P. Riesterer, A. Prokop, K. Merz and N. Metzler-Nolte, *Chem. Sci.*, 2012, **3**, 2062–2072.
108 K. Yan, C.-N. Lok, K. Bierla and C.-M. Che, *Chem. Commun.*, 2010, **46**, 7691–7693.
109 I. Ott, T. Koch, H. Shorafa, Z. Bai, D. Poeckel, D. Steinhilber and R. Gust, *Org. Biomol. Chem.*, 2005, **3**, 2282–2286.
110 C. Nardon, G. Boscutti and D. Fregona, *Anticancer Res.*, 2014, **34**, 487–492.
111 Y. Lu, X. Ma, X. Chang, Z. Liang, L. Lv, M. Shan, Q. Lu, Z. Wen, R. Gust and W. Liu, *Chem. Soc. Rev.*, 2022, **51**, 5518–5556.
112 (*a*) S. Raju, S. Sharangi, H. B. Singh, R. S. Prabhuraj, R. Srivastava, R. J. Butcher and S. Kumar, CCDC 2303816: Experimental Crystal Structure Determination, 2025, DOI: **10.5517/ccdc.csd.cc2hb9nt**; (*b*) S. Raju, S. Sharangi, H. B. Singh, R. S. Prabhuraj, R. Srivastava, R. J. Butcher and S. Kumar, CCDC 2303817: Experimental Crystal Structure Determination, 2025, DOI: **10.5517/ccdc.csd.cc2hb9pv**; (*c*) S. Raju, S. Sharangi, H. B. Singh, R. S. Prabhuraj, R. Srivastava, R. J. Butcher and S. Kumar, CCDC 2303818: Experimental Crystal Structure Determination, 2025, DOI: **10.5517/ccdc.csd.cc2hb9qw**; (*d*) S. Raju, S. Sharangi, H. B. Singh, R. S. Prabhuraj, R. Srivastava, R. J. Butcher and S. Kumar, CCDC 2303819: Experimental Crystal Structure Determination, 2025, DOI: **10.5517/ccdc.csd.cc2hb9rx**; (*e*) S. Raju, S. Sharangi, H. B. Singh, R. S. Prabhuraj, R. Srivastava, R. J. Butcher and S. Kumar, CCDC 2303820: Experimental Crystal Structure Determination, 2025, DOI: **10.5517/ccdc.csd.cc2hb9sy**; (*f*) S. Raju, S. Sharangi, H. B. Singh, R. S. Prabhuraj, R. Srivastava, R. J. Butcher and S. Kumar, CCDC 2303821: Experimental Crystal Structure Determination, 2025, DOI: **10.5517/ccdc.csd.cc2hb9tz**; (*g*) S. Raju, S. Sharangi, H. B. Singh, R. S. Prabhuraj, R. Srivastava, R. J. Butcher and S. Kumar, CCDC 2303822: Experimental Crystal Structure Determination, 2025, DOI: **10.5517/ccdc.csd.cc2hb9v0**; (*h*) S. Raju, S. Sharangi, H. B. Singh, R. S. Prabhuraj, R. Srivastava, R. J. Butcher and S. Kumar, CCDC 2303823: Experimental Crystal Structure Determination, 2025, DOI: **10.5517/ccdc.csd.cc2hb9w1**.